Acta Crystallographica Section F
Structural Biology and Crystallization Communications
ISSN 1744-3091

Structure of 3-oxoacyl-(acyl-carrier protein) synthase II from *Thermus thermophilus* HB8

Bagautdin Bagautdinov,[a]* Yoko Ukita,[a] Masashi Miyano[b] and Naoki Kunishima[a]

[a]Advanced Protein Crystallography Research Group, RIKEN SPring-8 Center, Harima Institute, 1-1-1 Kouto, Sayo-cho, Sayo-gun, Hyogo 679-5148, Japan, and [b]Structural Biophysics Laboratory, RIKEN SPring-8 Center, Harima Institute, 1-1-1 Kouto, Sayo-cho, Sayo-gun, Hyogo 679-5148, Japan

Correspondence e-mail: bagautdi@spring8.or.jp

Received 21 February 2008
Accepted 15 April 2008

PDB Reference: *Tt*KAS II, 1j3n, r1j3nsf.

The β-ketoacyl-(acyl carrier protein) synthases (β-keto-ACP synthases; KAS) catalyse the addition of two-carbon units to the growing acyl chain during the elongation phase of fatty-acid synthesis. As key regulators of bacterial fatty-acid synthesis, they are promising targets for the development of new antibacterial agents. The crystal structure of 3-oxoacyl-ACP synthase II from *Thermus thermophilus* HB8 (*Tt*KAS II) has been solved by molecular replacement and refined at 2.0 Å resolution. The crystal is orthorhombic, space group $P2_12_12$, with unit-cell parameters a = 72.07, b = 185.57, c = 62.52 Å, and contains one homodimer in the asymmetric unit. The subunits adopt the well known α-β-α-β-α thiolase fold that is common to ACP synthases. The structural and sequence similarities of *Tt*KAS II to KAS I and KAS II enzymes of known structure from other sources support the hypothesis of comparable enzymatic activity. The dimeric state of *Tt*KAS II is important to create each fatty-acid-binding pocket. Closer examination of KAS structures reveals that compared with other KAS structures in the apo form, the active site of *Tt*KAS II is more accessible because of the 'open' conformation of the Phe396 side chain.

1. Introduction

Saturated fatty acids are the main stores of chemical energy in organisms and their synthesis is essential in all organisms except archaea. The synthesis of fatty acids occurs by multistep chemical reactions that are essentially the same in all organisms. In mammals, each fatty-acid synthesis reaction is catalyzed by a distinct domain of large multifunctional proteins (type I fatty-acid synthase; FAS), but in most bacteria and plant plastids it is catalyzed by a series of discrete proteins, each encoded by a separate gene, that catalyze discrete steps in chain elongation (type II FAS; Rock & Cronan, 1996).

3-Oxoacyl-(acyl-carrier protein) synthase II, also known as FabF or β-keto-ACP synthase II (KAS II), in concert with KAS I and KAS III, catalyzes the condensation reaction of fatty-acid synthesis by the transfer of two C atoms from malonyl-ACP to an acyl acceptor (Rock & Jackowski, 2002). The various species of KAS (KAS I, KAS II and KAS III) differ in amino-acid sequence, substrate chain-length specificity and sensitivity to the currently known inhibitors of fatty-acid synthases: cerulenin, thiolactomycin, platencin and platensimycin (Heath *et al.*, 2002; Wang *et al.*, 2006, 2007). The amino-acid sequences of KAS I and KAS II share 38% identity and their functions are closely related, catalyzing the condensation of acyl-ACP with malonyl-ACP. In plastids, KAS I extends C_4 in the substrate to C_{16} in six rounds of elongation, whereas KAS II carries out an additional step to give a C_{18} product (Olsen *et al.*, 2001). KAS III initiates fatty-acid synthesis and is specialized for the first elongation step from C_2 to C_4. It has only ~18% sequence identity to KAS I and KAS II and is selective for acetyl coenzyme A (acetyl-CoA) over acyl-ACP (Qiu *et al.*, 2001). KAS III is further distinguished by its His-Asn-Cys catalytic triad, in contrast to the His-His-Cys triad found in the KAS I and KAS II enzymes (Qiu *et al.*, 1999; Davies *et al.*, 2000; Olsen *et al.*, 1999; Huang *et al.*, 1998). Despite their differences in catalytic action, the three KAS enzymes show similarity in their core structure, suggesting that they are evolutionarily related.

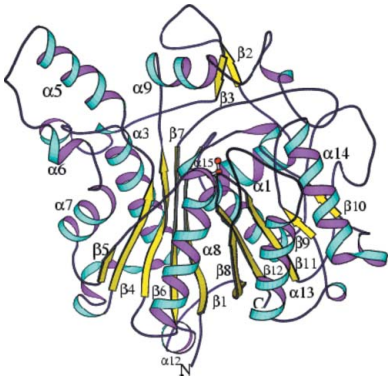

The KAS enzymes are considered as potential drug targets for the treatment of certain cancers and tuberculosis and may also be useful for modification of plant oils and polyketide engineering (Katz & Donadio, 1993). This has prompted interest in detailed studies of their structures. Crystal structures have been reported for the KAS enzymes *Ec*KAS I from *Escherichia coli* (Olsen *et al.*, 1999, 2001; Pappenberger *et al.*, 2007), *Ec*KAS II from *E. coli* (Huang *et al.*, 1998; Wang *et al.*, 2006), *Ss*KAS II from *Synechocystis* sp. (Moche *et al.*, 2001), *Sp*KAS II from *Streptococcus pneumoniae* (Price *et al.*, 2003), *Mt*KAS II from *Mycobacterium tuberculosis* (Sridharan *et al.*, 2007), human mitochondrial *Hsmt*KAS (Christensen *et al.*, 2007), *Ec*KAS III from *E. coli* (Qiu *et al.*, 1999, 2001; Davies *et al.*, 2000) and *Mt*KAS III from *M. tuberculosis* (Scarsdale *et al.*, 2001; Musayev *et al.*, 2005). These studies of members of the KAS family have provided valuable information on the mechanism of action of the enzymes. It was found that the fatty-acid synthase inhibitor cerulenin selectively targets KAS I and KAS II and forms a covalent bond with the cysteine in the active site of the enzymes, with its tail occupying the long hydrophobic cavity that normally contains the growing acyl chain of the natural substrate (Kauppinen *et al.*, 1988; Price *et al.*, 2001). Thiolactomycin and its analogues inhibit all three KAS enzymes and bind to the malonate portion of the active site (Omura *et al.*, 1983; Dolak *et al.*, 1986). Platencin targets KAS II and KAS III, while platensimycin is the most potent inhibitor reported for KAS I and KAS II; its action is based on competition with malonyl-ACP for the malonyl subsite of the enzyme (Wang *et al.*, 2006, 2007). Recently, a synthetic small molecule, 2-phenylamino-4-methyl-5-acetylthiazole, that binds to the active site of *Ec*KAS I has been identified (Pappenberger *et al.*, 2007).

The KAS structures reveal flexible regions in the active-site tunnel which may undergo conformational changes to allow the entrance and transfer of substrates at the various reaction stages. Of particular interest is the role of the phenylalanine close to the active-site cysteine, the side chain which undergoes considerable conformational changes to facilitate transfer of the substrates depending on the stage of catalysis. To clarify the details relating to the architecture of the active site which may be important in the reaction pathway, we have determined the crystal structure of 3-oxoacyl-ACP synthase II from the thermophilic organism *Thermus thermophilus* (*Tt*KAS II) at 2.0 Å resolution and discuss the enzymatic activity based on sequence and structural comparisons with other KASs. Although most of the structural details are similar in *Tt*KAS II and other KAS I and KAS II enzymes, some notable changes were found in the present structure. The side-chain conformation of Phe396 in the apo *Tt*KAS II is more 'open' compared with the analogous phenylalanine in other apo KASs. Such regions may undergo fewer conformational changes to facilitate movement of the substrates and reaction products and therefore may be more sensitive to substrates as well as to inhibitors. To gain knowledge of the possible interactions between *Tt*KAS II and fatty-acid synthase inhibitors, the *Tt*KAS II structure was compared with known liganded KAS structures.

2. Materials and methods

2.1. Protein expression and purification

The 3-oxoacyl-ACP synthase II from *T. thermophilus* HB8 (TTHA0413) used in this study has a molecular weight of 43.2 kDa and consists of 408 amino-acid residues. The plasmid was digested with *Nde*I and *Bgl*II and the fragment was inserted into the expression vector pET-11a (Novagen) linearized with *Nde*I and *Bam*HI. *E. coli* BL21 Codon Plus (DE3)-RIL cells were transformed with the recombinant plasmid and grown at 310 K in Luria–Bertani medium containing 50 µg ml^{-1} ampicillin for 20 h. The cells were harvested by centrifugation at 4500*g* for 5 min at 277 K, suspended in 20 m*M* Tris–HCl pH 8.0 containing 0.5 *M* NaCl, 5 m*M* 2-mercaptoethanol and 1 m*M* phenylmethylsulfonyl fluoride and finally disrupted by sonication and heated at 363 K for 10 min. The cell debris and heat-denaturated proteins were removed by centrifugation at 20 000*g* for 30 min. The supernatant solution was used as the crude extract for purification. The crude extract was desalted on a HiPrep 26/10 desalting column (Amersham Biosciences) and applied onto a Super Q Toyopearl 650 M (Tosoh) column equilibrated with 20 m*M* Tris–HCl pH 8.0 (buffer *A*). After elution with a linear gradient of 0–0.3 *M* NaCl, the fraction containing protein was desalted with a HiPrep 26/10 desalting column in 10 m*M* potassium phosphate pH 7.0. The sample was then applied onto a Bio-Scale CHT-20-I column (Bio-Rad) equilibrated with 10 m*M* potassium phosphate pH 7.0 and eluted with a linear gradient of 10–300 m*M* potassium phosphate pH 7.0. The sample was concentrated by ultrafiltration (Vivaspin, 5 kDa cutoff) and loaded onto a HiLoad 16/60 Superdex 200 prep-grade column (Amersham Biosciences) equilibrated with buffer *A* containing 0.2 *M* NaCl. The homogeneity and identity of the purified sample were assessed by SDS–PAGE (Laemmli, 1970) and N-terminal sequence analysis. Finally, the purified protein was concentrated to 18.0 mg ml^{-1} using ultrafiltration and stored at 203 K.

2.2. Protein crystallization

Crystallization trials were carried out using the oil-microbatch method (Chayen *et al.*, 1990) in Nunc HLA plates at 291 K using a TERA crystallization robot with a proprietary set of crystallization screening reagents (Sugahara & Miyano, 2002). 0.5 µl screen solution was mixed with 0.5 µl protein solution (protein concentration of 18.0 mg ml^{-1} in 20 m*M* Tris–HCl pH 8.0 and 50 m*M* sodium chloride). The crystallization drop was overlaid with a 1:1 mixture of silicone and paraffin oil (13 µl). One condition yielded thin plate-shaped crystals of approximate dimensions 0.2 × 0.1 × 0.03 mm. These crystals appeared about a month after setup. The precipitant solution consisted of 25%(*w*/*v*) PEG 4000, 0.05 *M* magnesium chloride and 100 µl sodium citrate pH 5.3.

2.3. Data collection and processing

X-ray diffraction-intensity data were collected on SPring-8 beamline BL45XU using a Rigaku R-AXIS V imaging-plate detector. Prior to data collection, the crystals were flash-cooled in a cryoprotectant solution consisting of the precipitant solution diluted with glycerol at 30%(*v*/*v*). A total of 180 frames were collected with 1° oscillation and 30 s exposure time per image. The wavelength of the synchrotron radiation was 0.9 Å and the crystal-to-detector distance was 200 mm. The diffraction data were integrated and scaled to 2.0 Å resolution using *DENZO* and *SCALEPACK* as implemented in the *HKL*-2000 program package (Otwinowski & Minor, 1997). Table 1 summarizes the data-collection and processing statistics.

2.4. Structure determination and refinement

The crystals belong to space group $P2_12_12$, with unit-cell parameters a = 72.07, b = 185.57, c = 62.52 Å. Assuming the presence of two 3-oxoacyl-ACP synthase II molecules in the asymmetric unit, the Matthews coefficient V_M (Matthews, 1968) was calculated to be the reasonable value 2.42 Å^3 Da^{-1}, corresponding to a solvent content of 49.1%. The structure was solved by the molecular-replacement method implemented in the *CNS* package (Brünger *et al.*, 1998). The structure of *Ss*KAS II (PDB code 1e5m; Moche *et al.*, 2001) was used

as a search model. Structure factors in the resolution range 15.0–4.0 Å were used for both the cross-rotation and translation searches. The data set gave clear translation-search solutions, with the two largest monitor values being 0.226 and 0.225, which were 2σ units above the mean value of 0.111 (σ = 0.057); the strongest cross-rotation peaks had values of 0.0643 and 0.0604, which were 4.2σ above the mean value of 0.0165 (σ = 0.0113). The dimeric search model gave a significant monitor value of 0.453 for the translation search, which was 3σ above the mean value of 0.219 (σ = 0.080). The dimer-search peak was consistent with one of the two highest peaks from the monomer search. Rigid-body refinement was then used to improve the initial phases derived from the dimer model. Electron-

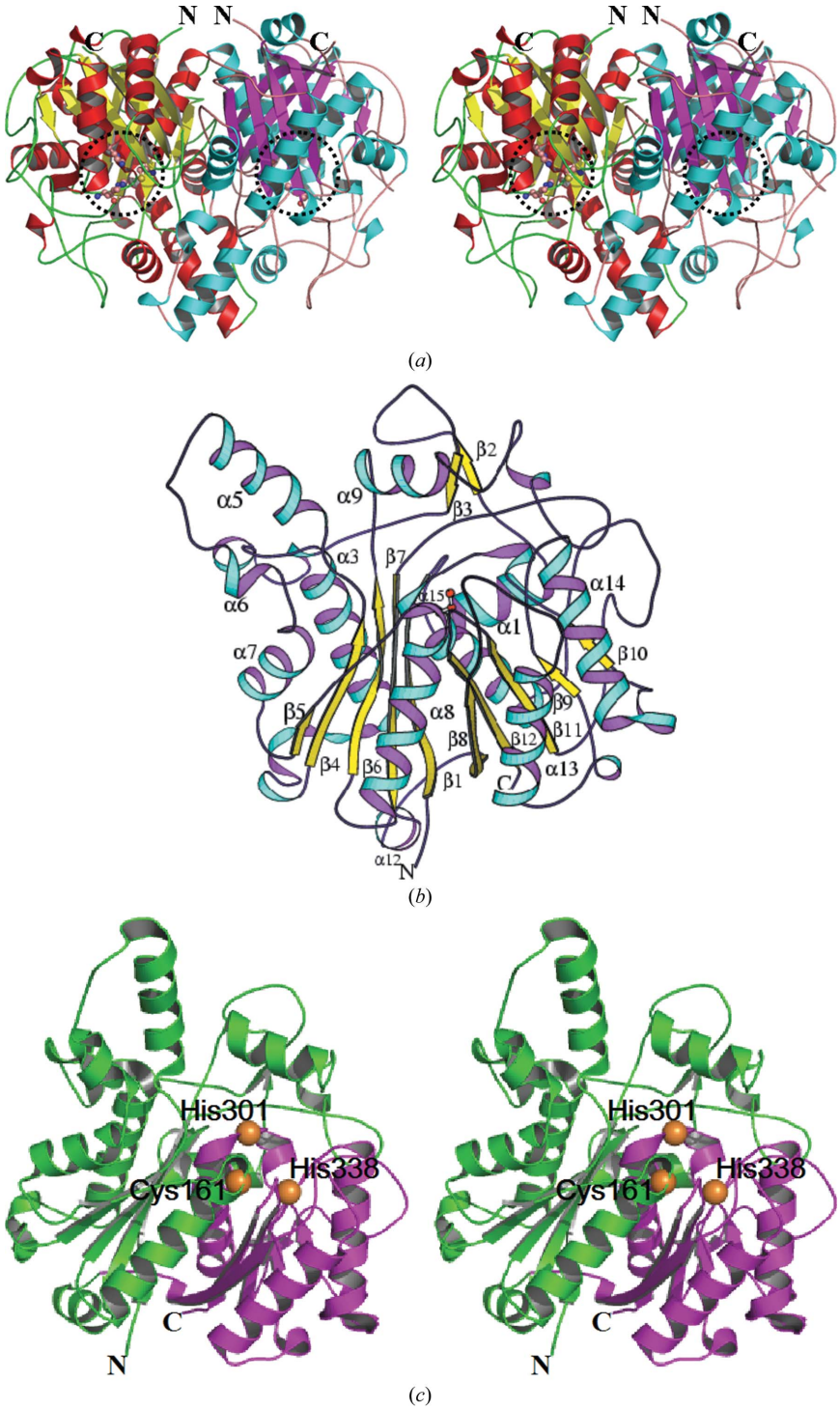

Figure 1
Structure of *Tt*KAS II. (*a*) Ribbon stereo diagram of the dimeric arrangement of *Tt*KAS II. One subunit is shown in cyan (helices) and magenta (strands) and the other is shown in red (helices) and yellow (strands). The active-site residues Cys161, His301 and His338 are shown as ball-and-stick models. Dashed circles indicate the location of the active site in each subunit. (*b*) Ribbon diagram of the *Tt*KAS II subunit with labelling of secondary-structure elements. The secondary-structure assignment was performed using the Kabsch–Sander algorithm (Kabsch & Sander, 1983). Cys161 in the N-terminus of α8 is shown as a ball-and-stick model. (*c*) A stereoview of the *Tt*KAS II subunit. The N- and C-terminal halves are shown in green and magenta, respectively. The positions of the active-site residues Cys161, His301 and His338 are shown as orange spheres.

Table 1
Diffraction data and structural refinement statistics.

Values in parentheses are for the highest resolution shell.

Crystal data	
Space group	$P2_12_12$
Unit-cell parameters (Å)	a = 72.067, b = 185.573, c = 62.517
Subunits per ASU	2
Data collection and refinement	
Temperature (K)	100
Wavelength (Å)	0.9
Resolution range (Å)	30–2.0 (2.07–2.0)
No. of unique reflections	56133 (4619)
Redundancy	4.8 (4.4)
Completeness (%)	97.7 (81.1)
Mean $I/\sigma(I)$	16.1 (4.2)
R_{merge}† (%)	9.5 (23.5)
No. of protein atoms	6080
No. of water molecules	462
Mean B factor (Å^2)	28.40
Mean B factor, main chains (Å^2)	26.5
Mean B factor, side chains (Å^2)	29.9
Mean B factor, waters (Å^2)	35.94
R_{work}‡/R_{free}§	0.210/0.258
Ramachandran plot (%)	
Most favoured	89.7
Additionally allowed	9.4
Generously allowed	0.6
Disallowed	0.3
PDB code	1j3n

† $R_{merge} = \sum_{hkl}\sum_i |I_i(hkl) - \langle I(hkl)\rangle| / \sum_{hkl}\sum_i I_i(hkl)$, where $I_i(hkl)$ and $\langle I(hkl)\rangle$ are the observed intensity of measurement i and the mean intensity of the reflection with indices hkl, respectively. ‡ $R_{work} = \sum |F_{obs} - F_{calc}| / \sum F_{obs}$, where F_{obs} and F_{calc} are the observed and calculated structure factors, respectively. § R_{free} is the R factor for a subset of 5% of the reflections that were omitted from refinement.

density maps were viewed with *TURBO-FRODO* (Roussel & Cambillau, 1992) and showed clear densities for both monomers. The initial model was rebuilt with the correct sequence and subjected to extensive cycles of NCS-restrained crystallographic refinement interspersed with visual inspection and manual adjustment. The final model of the structure was produced after several rounds of model building and energy minimization followed by individual B-factor refinement. Water molecules were added to the model and inspected manually during refinement. Models were refined with a citrate molecule and an Mg^{2+} ion. The progress of refinement was monitored using the cross-validation indicator R_{free} (Brünger, 1992), which was calculated using 5% of the reflections as a test set. The program *PROCHECK* (Laskowski *et al.*, 1993) was used for inspection and correction of the model within a refinement cycle. The last refinement of coordinates using the 30.0–2.0 Å resolution reflections resulted in R_{work} = 21.0% and R_{free} = 25.8%. The refinement statistics and the details of the final model are given in Table 1.

2.5. Quality of the model

The refined model contains 816 amino-acid residues, a citrate molecule, an Mg^{2+} ion and 463 well defined water molecules. In each subunit, Leu340 is in a disallowed Ramachandran conformation and Ala160 and Ser304 are in generously allowed conformations. They all have well resolved electron densities. The dihedral (φ, ψ) angles of Leu340 are 48° and −113°. Such a violation of the allowed Ramachandran conformation (positive φ, negative ψ) has been observed in several protein structures for the amino-acid residue at the i + 1 position of a type II′ β-turn and the unfavourable conformations of such residues are compensated by hydrogen bonds (Gunasekaran *et al.*, 1996). Analogously, in the current structure Leu340 adopts position i + 1 of a type II′ β-turn in the tight turn which connects strand β10 to helix α15.

The structures were superimposed on each other using the program *LSQKAB* (Kabsch, 1976) from the *CCP*4 package (Collaborative Computational Project, Number 4, 1994). The figures illustrating the structures were prepared with the programs *PyMOL* (DeLano, 2002), *MOLSCRIPT* (Kraulis, 1991) and *RASTER3D* (Merritt & Bacon, 1997). Sequence alignments were generated using *ClustalX* (Jeanmougin *et al.*, 1998). Electrostatic surface potentials were calculated using the vacuum electrostatics feature of *PyMOL* (DeLano, 2002).

3. Results and discussion

3.1. Overall structure

The crystal structure of *Tt*KAS II (space group $P2_12_12$) contains two independent molecules in the asymmetric unit. The pair of molecules around the noncrystallographic twofold-symmetry axis form a homodimer with a subunit size of 408 amino acids. In contrast, the hexagonal $P3_121$ structures of *Ec*KAS II (Huang *et al.*, 1998) and *Ss*KAS II (Moche *et al.*, 2001) crystallize with only one molecule in the asymmetric unit, but also reveal the presence of a tight dimer between subunits related by a crystallographic twofold axis. Ribbon diagrams of the homodimer and subunit of the *Tt*KAS II structure are shown in Fig. 1. Each subunit is composed of 12 β-strands and 15 α-helices. As with other condensing enzymes, the *Tt*KAS II molecule adopts the thiolase fold (Mathieu *et al.*, 1994), α-β-α-β-α, in which each α comprises two α-helices and each β is made up of a five-stranded mixed β-sheet (Figs. 1*b* and 2). The additional structural elements that cover short stretches of residues in the polypeptide chain of *Tt*KAS II do not perturb the general fold. Each subunit contains two halves, residues 1–249 (N-terminal domain) and 250–408 (C-terminal domain), which have similar structures related by the pseudo-twofold axis, except for the insertion and loop regions (Fig. 1*c*). This is indicative of protein generation through gene duplication. The N-terminal domain of the subunit forms a capping region and the C-terminal domain defines a highly structured core.

The dimerization of the subunits creates an extensive interface region. A total of 19.1% or 2857 Å^2 of the accessible surface area of the subunits (15 040 Å^2) is buried in the interface. This is comparable with the buried areas in the crystallographic twofold homodimers of *Ec*KAS II (buried area 20% or 3030 Å^2; Huang *et al.*, 1998) and *Ss*KAS II (21% or 3175 Å^2; Moche *et al.*, 2001). The dimer interface contains a large number of water molecules forming a network of hydrogen bonds. The polar interactions between the two subunits are listed in Table 2. Most of the structural elements that participate in dimerization are located in the N-terminal half of the subunit and mainly consist of hydrophobic residues. The secondary-structure elements involved in dimerization include the loops between α2 and β3 and between β8 and α13, helices α6, α7 and α8 and strands β8 and β12. The residues of helices α6 and α7 from one subunit line the channel that leads to the active site of the other subunit. The close conservation of the positions of the secondary-structure elements of KAS I and KAS II are shown in Fig. 3 by C^α superposition of subunits of other KAS enzymes on that of *Tt*KAS II. The C^α superposition of the subunit structures of *Ss*KAS II, *Ec*KAS II and *Ec*KAS I on that of *Tt*KAS II resulted in root-mean-square deviations of 1.49, 1.69 and 3.52 Å, respectively. There are 105 residues (∼25%) that are conserved in all four structures presented in Fig. 3.

3.2. The active-site architecture of *Tt*KAS II

The active-site cysteine in KAS enzymes has been identified by sequence comparison (Siggaard-Andersen, 1993), mutagenesis (Joshi

et al., 1997) and structural studies (Moche *et al.*, 1999; Price *et al.*, 2001; Wang *et al.*, 2006; Sridharan *et al.*, 2007). The structure of *Ec*KAS II complexed with cerulenin, an irreversible covalent modifier that mimics the formation of the acyl-thioester, suggests that the catalytic residues in *Ec*KAS II are Cys163, His303 and His340 (Moche *et al.*, 1999). Alignment of the available KAS II and KAS I structures indicates that the residues of the Cys-His-His triad are appropriately positioned to function as the catalytic residues. The corresponding residues in the present *Tt*KAS II are Cys161, His301 and His338. Cys161 lies at the N-terminus of helix α8, allowing it to exploit the α-helix dipole moment and thereby become nucleophilic (Davies *et al.*, 2000). The nucleophilic cysteine of the active-site triad was required for acyl-enzyme formation and the overall condensation activity. His301 and His338 are 3.75 and 3.54 Å away from Cys161, respectively. The electrostatic potential surface of the *Tt*KAS II subunit is shown in Fig. 4. The bottom of the active site where the catalytic Cys161 is located is mainly hydrophobic. In KAS I and KAS II the active site is divided in half, one half for acyl-enzyme formation and the other half for malonyl binding (Davies *et al.*, 2000). KAS III lacks an acyl-binding pocket since it is only required to bind a methyl group. The distance between the two active-site Cys161 residues in the dimer is 24.7 Å (Fig. 1*a*). The residues closer than half of this distance to Cys161 create a crevice. The crevice is lined by β8 (Glu255 and Asp263), the β8–α13 loop (His266, Thr268 and Pro270), the loop between β9 and α14 (Thr303 and Pro306), residues from α14 (Pro306, Val307, Gly308, Ala311 and Glu312), the β10–α15 loop (Lys333 and His338) and the β-hairpin motif including the β11–β12 loop (Phe394 and Gly398) and β12 (His399 and Asn400). The active-site cavity is mainly formed by residues from the C-terminal half of one subunit of the dimer, but residues from the N-terminal half between α6 and α7 (Ile132–Ser142) of the other subunit form part of the cavity wall. Thus, the dimer formation observed in the enzymes plays a role in the complete formation of the fatty-acid binding pocket. Based on these structure data and the similarity to the *Ec*KAS II dimer, which has been shown to be dimeric both in solution and in the crystal structure (Huang *et al.*, 1998), the homodimer observed in the asymmetric unit is the functional assembly of *Tt*KAS II. Most of the residues positioned at the entrance to the active-site cavity are strictly conserved

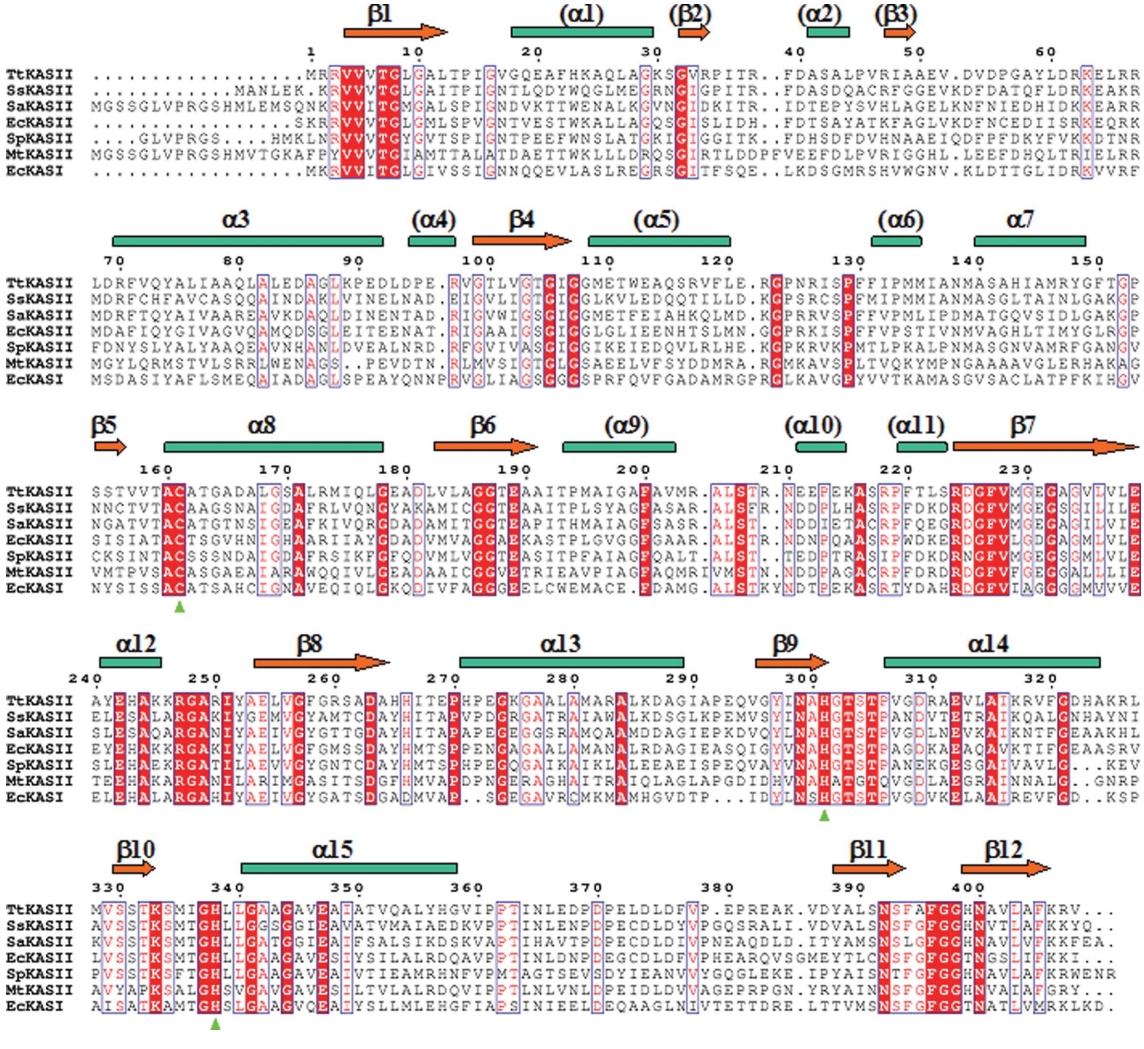

Figure 2
Sequence alignment of KAS I and II from selected organisms. The β-strands (drawn as orange arrows) and α-helices (drawn as lime rectangles) of *Tt*KAS II are shown with assigned labels above the sequences. Secondary-structural elements that are outside the thiolase-fold core are shown in parentheses. Conserved amino-acid residues are coloured red. The catalytic triad residues are marked with green triangles. The sequences used in this figure were obtained from the PDB: *Ss*KAS II, 1e5m (Moche *et al.*, 2001); *Ec*KAS II, 1kas (Huang *et al.*, 1998); *Sa*KAS II, 2gqd (Miller *et al.*, unpublished work); *Sp*KAS II, 1oxh (Price *et al.*, 2003); *Mt*KAS II, 2gp6 (Sridharan *et al.*, 2007); *Ec*KAS I, 1dd8 (Olsen *et al.*, 1999).

in KAS I and KAS II (Fig. 2), indicating the essential structural identity of the crevice regions of these enzymes.

In addition to the Cys161–His301–His338 triad, important residues within the active site include the conserved Phe227, Lys333, Ile106, which is flexible on cerulenin binding, and two main-chain amides belonging to Cys161 and Phe396 that constitute an oxyanion hole adjacent to the cysteine (Fig. 5). In subunits *A* and *B* water molecules (Wat23 and Wat8, respectively) are hydrogen bonded to the backbone carbonyl O atom of Cys161. As a water molecule is conserved in this position in other KAS II enzymes (Olsen *et al.*, 2004; Sridharan *et al.*, 2007), it may play a structural role such as orienting or maintaining the position of Cys161 in the active site. The side chains of the two histidines His301 and His338 point towards Cys161. In KAS enzymes, the active-site histidines have different electronic states and functions (Zhang *et al.*, 2006). His301 NE forms a hydrogen bond to a structured water molecule (Wat326 in subunit *A* and Wat441 in subunit *B*). Other KAS structures (Huang *et al.*, 1998; Price *et al.*, 2003; Olsen *et al.*, 1999) reveal water molecules in a very similar location to Wat326 (Wat441) that are hydrogen bonded to the equivalent histidines. His338 makes a hydrogen bond to Cys161 SG and may extract the Cys161 proton.

Therefore, analogous to other KAS enzymes, the protonated NE atom of His338 in *Tt*KAS II may stabilize the negative charge developed on the malonyl thioester carbonyl in the transition state. His301 NE accelerates catalysis by deprotonating a structured active-site water for nucleophilic attack on the C3 of malonate, releasing bicarbonate.

The positive charge on the conserved Lys333 is 3.36 Å from His301 ND and thus may control the electronic state of His301. Phe396 functions as a 'gatekeeper' that controls the order of substrate addition. In the cerulenin complex of *Ec*KAS II, Ile108 (equivalent to Ile106 in *Tt*KAS II), which is located on the floor of the cerulenin-binding tunnel, takes on a new rotameric form (Moche *et al.*, 1999), while in *Ec*KAS I Ile108 is replaced by a Gly, which allows cerulenin easy access into the tunnel. These data have been used to explain the higher sensitivity of KAS I to inhibition by cerulenin compared with KAS II (Price *et al.*, 2001; Val *et al.*, 2000). The residues Leu340, which is in a disallowed conformation, and Ala160 and Ser304, which are in generously allowed conformations, are located close to the active-site triad Cys161–His301–His338. The similarly distorted Leu and Ala near the active-site residues are characteristic of KAS I and KAS II and might be important for formation of the active site (Huang *et al.*, 1998; Moche *et al.*, 2001).

Table 2
Hydrogen-bonding interactions between the *A* and *B* subunits of the dimer.

The maximum distance cutoff between contact atoms is 3.5 Å.

Protein atom, subunit *A*	Protein atom, subunit *B*	Distance (Å)
Ala43 O	Asn125 ND2	3.29
Glu96 O	Arg263 NH2	2.67
Asn125 ND2	Ala43 O	3.26
Asn138 OD1	His399 NE2	2.92
Asn138 O	His399 NE2	3.29
Thr151 O	Arg283 NH1	3.07
Thr151 O	Ala162 N	3.37
Ser154 O	His399 ND1	2.79
Ser155 OG	Asp166 OD2	3.14
Ser155 OG	Asp166 OD1	3.31
Thr156 O	Val158 N	2.93
Asp166 OD1	Ser155 OG	3.34
Asp166 OD2	Ser155 OG	2.79
Arg173 NE	Glu179 OE2	3.23
Arg173 NH2	Glu179 OE2	2.79
Glu179 OE2	Arg173 NH2	2.74
Glu179 OE2	Arg173 NE	3.15
Glu179 OE1	Arg260 NH2	3.16
Arg260 NH2	Glu179 OE1	2.86
Arg262 N	Thr151 O	3.17
Arg262 N	Gly152 O	3.47
Arg283 NH2	Glu96 O	2.81
Arg283 NH1	Thr151 O	3.04
His399 ND1	Ser154 O	3.04
His399 ND1	Ser154 OG	3.38

3.3. Flexibility of the active-site region

In an effort to obtain further information about the active site, the *Tt*KAS II structure was superposed on the structures of the complexes of *Ec*KAS II with cerulenin (Moche *et al.*, 1999) and with platensimycin (Wang *et al.*, 2006) and of *Ec*KAS I with thiolactomycin (Price *et al.*, 2001) (Fig. 6). Cerulenin resides in the acyl-binding hydrophobic tunnel of KAS I and KAS II (Moche *et al.*, 1999; Price *et al.*, 2001), while thiolactomycin and platensimycin bind to the malonate portion of the active site (Price *et al.*, 2001; Wang *et al.*, 2006). The crystal structures of *Ec*KAS II in complex with cerulenin (Moche *et al.*, 1999) and with lauroyl-CoA, a mimic of the natural acyl-ACP substrate (Wang *et al.*, 2006), revealed a rotamer conformation

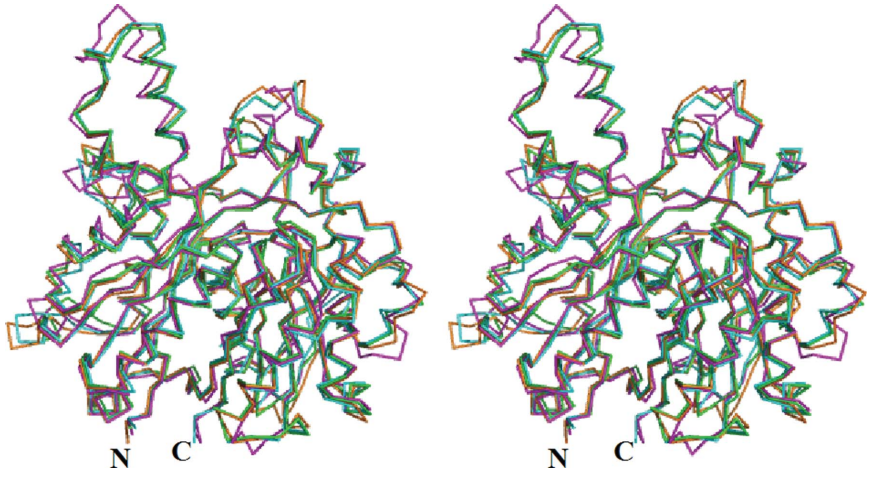

Figure 3
A stereoview of the superposed C^{α} traces of the subunits of *Tt*KAS II (green), *Ss*KAS II (PDB code 1e5m; Moche *et al.*, 2001; cyan), *Ec*KAS II (PDB code 1kas; Huang *et al.*, 1998; orange) and *Ec*KAS I (PDB code 1dd8; Olsen *et al.*, 1999; magenta).

change of Phe400 and Ile108 to accommodate the substrates. A similar conformational change of Phe400 was also observed in *Ec*KAS II with platensimycin and with mutation C163Q. The corresponding phenylalanine (Phe392 in *Ec*KAS I) in the structures of *Ec*KAS I upon formation of the acyl-enzyme intermediate (Olsen *et al.*, 2001) and in complex with cerulenin (Price *et al.*, 2001) shows similar movements. This shift swings phenylalanine into an 'open' conformation which is necessary because in the apo state this conformation occupies the space of the KAS reaction intermediate. The related Phe396 in the present unliganded *Tt*KAS II has a conformation that is intermediate between the 'open' and 'closed' conformations in *Ec*KAS II (Fig. 6). Other available crystal structures for KAS show that in the apo state the phenylalanine is in a closed conformation serving as a lid that protects the active-site cavity from the solvent. In these KAS enzymes the flexible phenylalanine is flanked by conserved glycine residues, but in *Tt*KAS II it is flanked by alanine and glycine residues (Fig. 2).

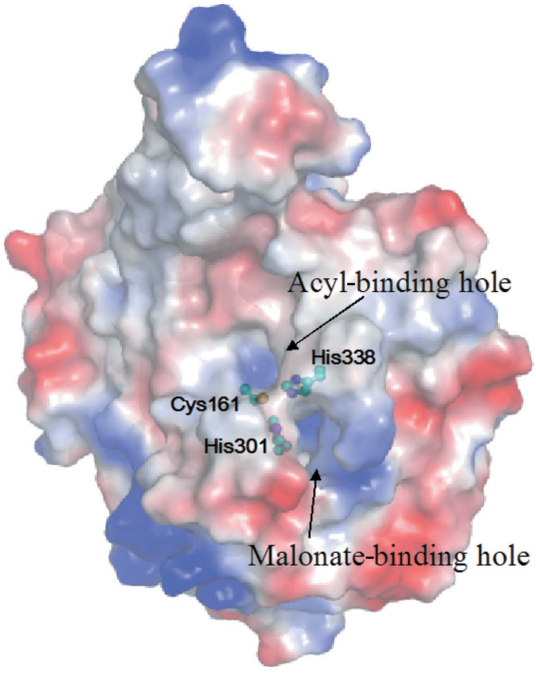

Figure 4
Surface-charge distribution of *Tt*KAS II viewed towards the active site. The electrostatic potential surface was calculated using only one subunit. Red indicates negative potential and blue positive potential. The active-site triad residues are shown as ball-and-stick models. Acyl- and malonate-binding holes are indicated.

Superposition of the structures of *Tt*KAS II and of *Ec*KAS II complexed with cerulenin, thiolactomycin and platensimycin reveals that for *Tt*KAS II to bind these inhibitors, the side chain of Phe396 should convert to a more 'open' conformation. The positional conservation of catalytic residues in the active sites of the superposed structures may indicate that these ligands would be able to fit into the active site of the present *Tt*KAS II, possibly with only minor conformational changes in the active-site tunnel, and to occupy a similar area and volume to those in *Ec*KAS I and II.

4. Conclusion

The structure analysis of *Tt*KAS II is consistent with the model for the catalytic mechanism of the elongation-condensing enzymes (Zhang *et al.*, 2006). The nucleophilicity of Cys161 is enhanced by the strong α8-helix dipole effect and the oxyanion hole formed by the backbone amides of Cys161 and Phe396 promotes the reaction by accommodating the negative charge on the thioester carbonyl that develops in the tetrahedral transition state. ACP is released and malonyl-ACP binds to the acyl-enzyme intermediate. His301 acti-

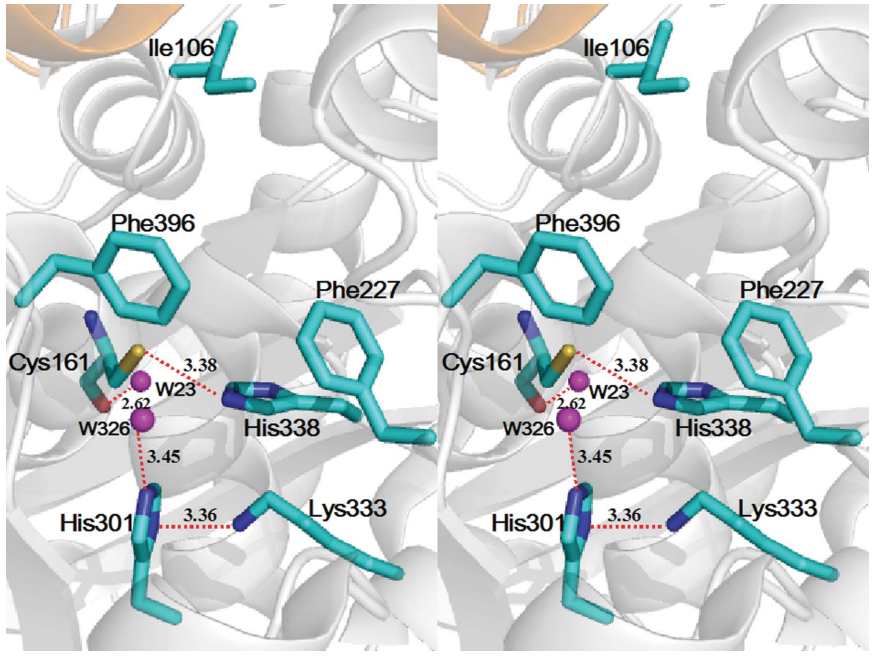

Figure 5
A stereoview of the *Tt*KAS II active site, illustrating the orientation of the key residues considered in this study. Subunits are represented by transparent ribbons and are shown in different colours. The back sides of important residues are shown as cyan stick models and water molecules are shown as magenta spheres. Cys161 is presented with main-chain atoms in order to visualize the hydrogen bond between the backbone carbonyl O atom and the nearby water molecule. The red dots show hydrogen-bond interactions.

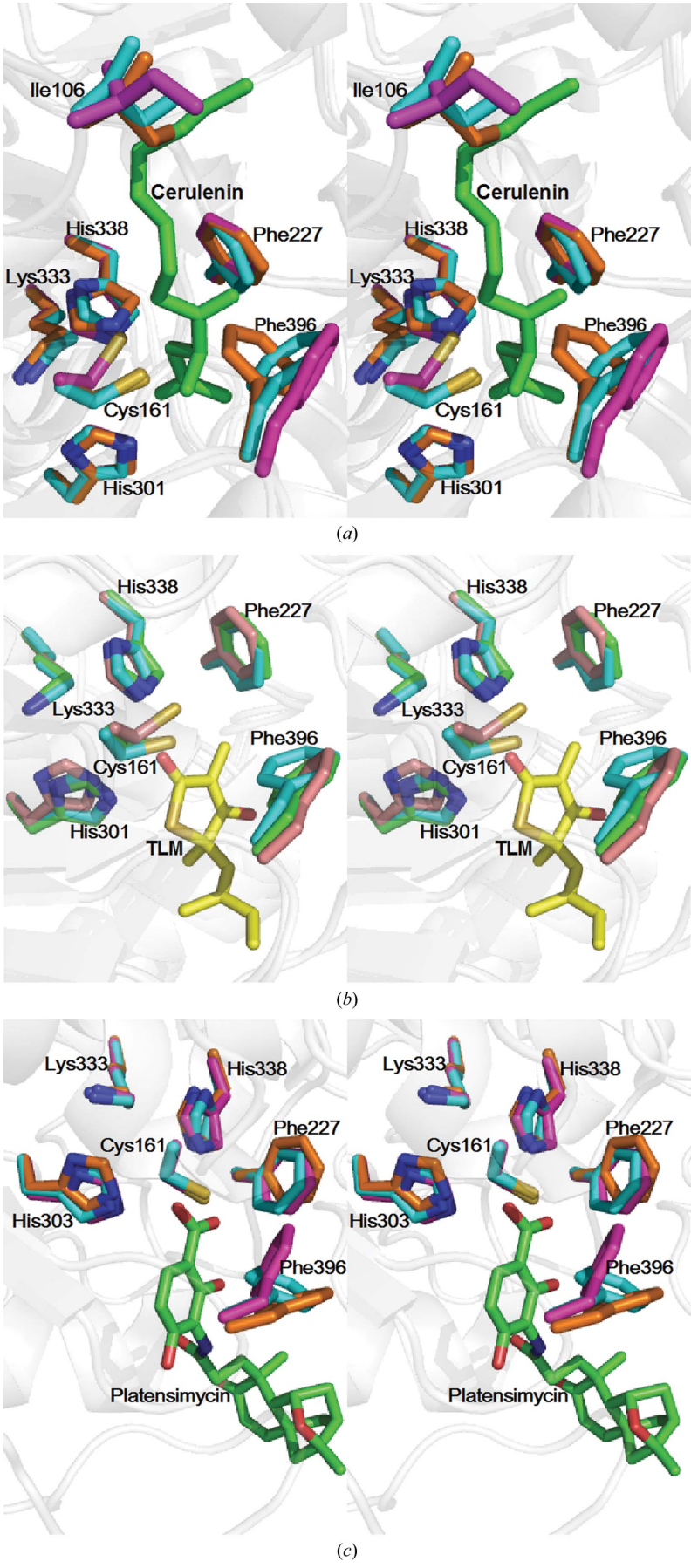

vates a structured catalytic water molecule Wat326 (Wat441) to attack the carboxylate of the malonyl-ACP and His338 acts as a second oxyanion hole that promotes the formation of the carbanion at the C2 of the malonate by stabilizing the enoyl intermediate.

Since the orientation of conserved catalytic residues, with the exception of Phe396, in the *Tt*KAS II structure is similar to that in *Ec*KAS II and because the active-site cavity may accommodate ligands as in *Ec*KAS II with minor conformational changes, we infer that the catalytic mechanisms of the two enzymes may also be very similar. The observed more open conformation of the gateway residue Phe396 in the apo state compared with other KAS enzymes may result in a higher sensitivity of *Tt*KAS II to known KAS inhibitors. The availability of coordinates for *Tt*KAS II also provides a basis for a structure-assisted search for new bacterial fatty-acid synthesis inhibitors.

The authors would like to thank the staff of RIKEN Genomic Sciences Center for providing the plasmid. We are also grateful to the beamline staff at beamline BL45XU of SPring-8 and Dr I. D. Brown (McMaster University, Canada) for critical reading of the manuscript. This work (TTHA0413/HTPF00003) was supported by the 'National Project on Protein Structural and Functional Analyses' funded by the MEXT of Japan.

References

Brünger, A. T. (1992). *Nature (London)*, **355**, 472–474.

Brünger, A. T., Adams, P. D., Clore, G. M., DeLano, W. L., Gros, P., Grosse-Kunstleve, R. W., Jiang, J.-S., Kuszewski, J., Nilges, M., Pannu, N. S., Read, R. J., Rice, L. M., Simonson, T. & Warren, G. L. (1998). *Acta Cryst.* D**54**, 905–921.

Figure 6
Active-site conformations of KAS enzymes. (*a*) Stereoview of the superposed active sites of the current apo *Tt*KAS II structure (cyan), apo *Ec*KAS II (orange; Huang *et al.*, 1998) and the complex between *Ec*KAS II and cerulenin (magenta; Moche *et al.*, 1999). Cerulenin is shown in green. *Ec*KAS I shows induced fit upon binding cerulenin. (*b*) Stereoview of the superposed active sites of *Tt*KAS II (cyan) and *Ec*KAS I in the apo form (PDB code 1dd8; Olsen *et al.*, 1999) and complexed with thiolactomycin (TLM; orange; PDB code 1fj4; Price *et al.*, 2001). TLM is shown in yellow. *Ec*KAS I shows no significant conformational changes upon binding TLM. (*c*) Stereoview of the superposed active sites of *Tt*KAS II (cyan) and *Ec*KAS II in the apo state (magenta; PDB code 2gfw; Wang *et al.*, 2006) and complexed with platensimycin (orange; PDB code 2gfx; Wang *et al.*, 2006).

Chayen, N. E., Shaw Stewart, P. D., Maeder, D. L. & Blow, D. M. (1990). *J. Appl. Cryst.* **23**, 297–302.
Christensen, C. E., Kragelund, B. B., von Wettstein-Knowles, P. & Henriksen, A. (2007). *Protein Sci.* **16**, 261–272.
Collaborative Computational Project, Number 4 (1994). *Acta Cryst.* D**50**, 760–763.
Davies, C., Heath, R. J., White, S. W. & Rock, C. O. (2000). *Structure*, **8**, 185–195.
DeLano, W. L. (2002). *The PyMOL Molecular Graphics System*. DeLano Scientific, San Carlos, California, USA.
Dolak, L., Castle, T., Truesdell, S. & Sebek, O. (1986). *J. Antibiot.* **39**, 26–31.
Gunasekaran, K., Ramakrishnan, C. & Balaram, P. (1996). *J. Mol. Biol.* **262**, 191–198.
Heath, R. J., White, S. W. & Rock, C. O. (2002). *Appl. Microbiol. Biotechnol.* **58**, 695–703.
Huang, W., Jia, J., Edwards, P., Denesh, K., Schneider, G. & Lindqvist, Y. (1998). *EMBO J.* **17**, 1183–1191.
Jeanmougin, F., Thompson, J. D., Gouy, M., Higgins, D. G. & Gibson, T. J. (1998). *Trends. Biochem. Sci.* **23**, 403–405.
Joshi, A. K., Witkowski, A. & Smith, S. (1997). *Biochemistry*, **36**, 2316–2322.
Kabsch, W. (1976). *Acta Cryst.* A**32**, 922–923.
Kabsch, W. & Sander, C. (1983). *Biopolymers*, **22**, 2577–2637.
Katz, L. & Donadio, S. (1993). *Annu. Rev. Microbiol.* **47**, 875–912.
Kauppinen, S., Siggaard-Andersen, M. & von Wettstein-Knowles, P. (1988). *Carlsberg Res. Commun.* **53**, 357–370.
Kraulis, P. J. (1991). *J. Appl. Cryst.* **24**, 946–950.
Laemmli, U. K. (1970). *Nature (London)*, **227**, 680–685.
Laskowski, R. A., MacArthur, M. W., Moss, D. S. & Thornton, J. M. (1993). *J. Appl. Cryst.* **26**, 283–291.
Mathieu, M., Zeelen, J., Pauptit, R. A., Erdmann, R., Kunau, W.-H. & Wierenga, R. K. (1994). *Structure*, **2**, 797–808.
Matthews, B. W. (1968). *J. Mol. Biol.* **33**, 491–497.
Merritt, E. A. & Bacon, D. J. (1997). *Methods Enzymol.* **277**, 505–524.
Moche, M., Dehesh, K., Edwards, P. & Lindqvist, Y. (2001). *J. Mol. Biol.* **305**, 491–503.
Moche, M., Schneider, G., Edwards, P., Denesh, K. & Lindqvist, Y. (1999). *J. Biol. Chem.* **274**, 6031–6034.
Musayev, F., Sachdeva, S., Scarsdale, J. N., Reynolds, K. A. & Wright, H. T. (2005). *J. Mol. Biol.* **346**, 1313–1321.
Olsen, J. G., Kadziola, A., von Wettstein-Knowles, P., Siggaard-Andersen, M. & Larsen, S. (2001). *Structure*, **9**, 233–243.
Olsen, J. G., Kadziola, A., von Wettstein-Knowles, P., Siggaard-Andersen, M., Lindqvist, Y. & Larsen, S. (1999). *FEBS Lett.* **460**, 46–52.
Olsen, J., Rasmussen, A., von Wettstein-Knowles, P. & Henriksen, A. (2004). *FEBS Lett.* **577**, 170–174.
Omura, S. I., Nakagawa, Y. A., Iwata, R., Takahashi, Y., Shimizu, H. & Tanaka, H. (1983). *J. Antibiot.* **36**, 109–114.
Otwinowski, Z. & Minor, W. (1997). *Methods Enzymol.* **276**, 307–326.
Pappenberger, G., Schulz-Gasch, T., Kusznir, E., Müller, F. & Hennig, M. (2007). *Acta Cryst.* D**63**, 1208–1216.
Price, A. C., Charles, O., Rock, C. O. & White, S. W. (2003). *J. Bacteriol.* **185**, 4136–4143.
Price, A. C., Choi, K.-H., Heath, R. J., Li, Z., White, S. W. & Rock, C. O. (2001). *J. Biol. Chem.* **276**, 6551–6559.
Qiu, X., Janson, C. A., Konstantinidis, A. K., Nwagwu, S., Silverman, C., Smith, W. W., Khandekar, S., Lonsdale, J. & Abdel-Megui, S. S. (1999). *J. Biol. Chem.* **274**, 36465–36471.
Qiu, X., Janson, C. A., Smith, W. W., Head, M., Lonsdale, J. & Konstantinidis, A. K. (2001). *J. Mol. Biol.* **307**, 341–356.
Rock, C. O. & Cronan, J. E. (1996). *Biochim. Biophys. Acta*, **1302**, 1–16.
Rock, C. O. & Jackowski, S. (2002). *Biochem. Biophys. Res. Commun.* **292**, 1155–1166.
Roussel, A. & Cambillau, C. (1992). *TURBO-FRODO*. Biographics and AFMB, Marseille, France.
Scarsdale, J. N., Kasanina, G., He, X., Reynolds, K. A. & Wright, T. (2001). *J. Biol. Chem.* **276**, 20516–20522.
Siggaard-Andersen, M. (1993). *Protein Sequence Data Anal.* **5**, 325–335.
Sridharan, S., Wang, L., Brown, A. K., Dover, L. G., Kremer, L., Besra, G. S. & Sacchettini, J. C. (2007). *J. Mol. Biol.* **366**, 469–480.
Sugahara, M. & Miyano, M. (2002). *Tanpakushitsu Kakusan Koso*, **47**, 1026–1032.
Val, D., Banu, G., Seshadri, K., Lindqvist, Y. & Dehesh, K. (2000). *Structure*, **8**, 565–566.
Wang, J. *et al.* (2006). *Nature (London)*, **441**, 358–361.
Wang, J. *et al.* (2007). *Proc. Natl Acad. Sci. USA*, **104**, 7612–7616.
Zhang, Y. M., Hurlbert, J., White, S. W. & Rock, C. O. (2006). *J. Biol. Chem.* **281**, 17390–17399.